Inorganic Chemistry
Article
pubs.acs.org/IC

Blue-Green Iridium(III) Emitter and Comprehensive Photophysical Elucidation of Heteroleptic Cyclometalated Iridium(III) Complexes

Kassio P. S. Zanoni,[†] Bruna K. Kariyazaki,[†] Akitaka Ito,[‡,§] M. Kyle Brennaman,[‡] Thomas J. Meyer,[‡] and Neyde Y. Murakami Iha*[,†]

[†]Laboratory of Photochemistry and Energy Conversion, Instituto de Química, Universidade de São Paulo − USP, Av. Prof. Lineu Prestes, 748, 05508-900, São Paulo, SP, Brazil

[‡]Department of Chemistry, University of North Carolina at Chapel Hill − UNC, 123 South Road, Chapel Hill, North Carolina 27599-3290, United States

[§]Department of Chemistry, Graduate School of Science, Osaka City University, 3-3-138 Sugimoto, Sumiyoshi-ku, Osaka 558-8585, Japan

Supporting Information

ABSTRACT: Synthesis and photophysical properties of the highly emissive complex $[Ir(Fppy)_2(dmb)]^+$ are reported along with those of additional heteroleptic cyclometalated Ir(III) complexes, $[Ir(ppy)_2(NN)](PF_6)$: *FppyH* = 2-(2,4-difluorophenyl)pyridine; *ppyH* = 2-phenylpyridine; NN = 4,4′-dimethyl-2,2′-bipyridine (*dmb*), 1,10-phenanthroline (*phen*), or 4,7-diphenyl-1,10-phenanthroline (*Ph₂phen*). TD-DFT calculations and Franck−Condon emission spectral band shape analyses show that the broad and structureless emission from $[Ir(Fppy)_2(dmb)]^+$ in acetonitrile at 298 K mainly arises from a triplet metal-to-ligand charge-transfer excited state, $^3MLCT_{Ir(ppy)\rightarrow NN}$. The emission maximum varies systematically with variations in electron-donating or -withdrawing substituents on both the *NN* and the *Xppy* ligands, and emission efficiencies are high, with an impressive $\phi \approx 1$ for $[Ir(Fppy)_2(dmb)]^+$. At 77 K in propionitrile/butyronitrile (4/5, v/v), emission from $[Ir(Fppy)_2(dmb)]^+$ is narrow and highly structured consistent with a triplet ligand-centered transition ($^3LC_{NN}$) and an inversion in excited-state ordering between the $^3MLCT_{Ir(ppy)\rightarrow NN}$ and $^3LC_{NN}$ states. In a semirigid film of the poly(ethyleneglycol)dimethacrylate with nine ethylene glycol spacers, PEG-DMA550, emission from $[Ir(Fppy)_2(dmb)]^+$ is MLCT-based. The thermal sensitivity of the photophysical properties of this excited state points to a possible application as a temperature sensor in addition to its more known use in light-emitting devices.

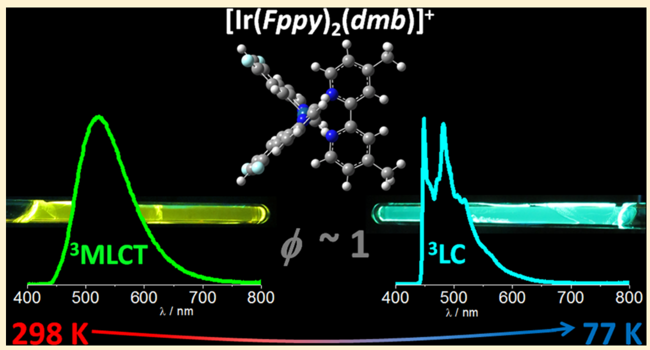

INTRODUCTION

Stable, emitting coordination compounds with tunable absorption and emission spectra and redox potentials have drawn worldwide attention due to their potential use in molecular devices.[1] In particular, Iridium(III) complexes have found application in oxygen sensors,[2] DNA intercalators,[3] luminescent biological probes,[4] CO_2 and water reduction,[1c,k,5] temperature sensors,[6] with the most appealing application as emitters in organic light-emitting diodes (OLEDs)[1b,k,7] and light-emitting electrochemical cells (LECs).[1c,8]

The photophysical properties of cyclometalated Ir(III) complexes are strongly influenced by spin−orbit coupling exerted by the Ir(III) core. For example, this leads to high triplet emission quantum yields due to the highly mixed spin character of the emitting excited states.[1c,i,9] The results of density functional theory (DFT) and time-dependent DFT (TD-DFT) studies show that their relatively short-lived emissions occur mainly from metal-to-ligand charge-transfer states (^{3}MLCT) with ligand-centered (^{3}LC) or mixed ^{3}MLCT/^{3}LC emissions being also possible depending on the complex and conditions.[10a−f] Heteroleptic 2-phenylpyridyl Ir(III) complexes, $[Ir(ppy)_2(NN)]^+$, have high photochemical and thermal stabilities, and the coordination chemistry is extensively based on a large number of ligands. Synthetic variations have been used to achieve comprehensive emission tuning over the entire visible region by incorporation of electron-donating or -withdrawing groups on both cyclometalated *ppy* and ancillary *NN* through their effect in stabilizing or destabilizing the donor and acceptor orbitals.[1c,10c,e,11] Excited-state properties of these complexes are also sensitive to the microenvironments around the complex (i.e., solvent polarity, rigidity, temperature) because of their

Received: January 10, 2014
Published: March 31, 2014

charge-transfer character and asymmetric structure,[12] with innumerous possibilities of emission colors.

Ligand and solvent variations have been used to develop the systematics of excited-state emission from this class of Ir(III) complexes. Further developments will benefit from a deeper understanding of the nature of the excited states and their emissive properties. In earlier work, we reported on the use of Re(I) complexes in PVK-based OLEDs.[1j,l] More recently, we proceeded to Ir(III) emitters, with the use of $[Ir(ppy)_2(dmb)]^+$, *ppyH* = 2-phenylpyridine and *dmb* = 4,4′-dimethyl-2,2′-bipyridine, as the active layer in a LEC for the first time.[13] This has motivated the engineering of new highly emissive compounds with appropriate characteristics for light-emitting devices and to obtain the synthetic control needed to tune excited-state properties. For this purpose, use of TD-DFT to provide insight into both electronic and molecular structure can be helpful. Quantitative tools for excited-state evaluation are also available by interpretation of excited-state properties including application of Franck−Condon (FC) analysis to emission spectra, which, through application of time-dependent perturbation theory and the Fermi "Golden Rule", provides quantitative understanding of time-dependent excited-state processes and has been applied to nonradiative decay in a series of Re(I), Os(II), and Ru(II) polypyridyl complexes.[12d,14]

In this Article, we report the synthesis of a blue-green highly emissive heteroleptic Ir(III) complex, $[Ir(Fppy)_2(dmb)]^+$, *FppyH* = 2-(2,4-difluorophenyl)pyridine, and its photophysical properties along with those of an additional three complexes of the type $[Ir(ppy)_2(NN)]^+$, *NN* = *dmb*, 1,10-phenanthroline (*phen*), or 4,7-diphenyl-1,10-phenanthroline (Ph_2phen), in different media and temperatures. $[Ir(Fppy)_2(dmb)]^+$ is novel in exhibiting an intense blue-green emission. Its emission properties, and those of the series of Ir(III) complexes, have been analyzed by Franck−Condon emission spectral fitting and TD-DFT calculations on the excited states. The effect of ligand substituents and medium effects on excited-state properties are rationalized systematically.

■ EXPERIMENTAL SECTION

All chemicals and solvents used for synthesis were purchased from Sigma-Aldrich or Synth, and were used as supplied. Spectroscopic or HPLC grade acetonitrile, propionitrile, and butyronitrile were used as supplied. For electrochemical measurements, acetonitrile was distilled prior to use.

^1H NMR spectra were recorded in a DRX500 (500 MHz) or in an AC200 (200 MHz) Bruker Avance spectrometer, using CD_2Cl_2, $CDCl_3$, or CD_3CN as solvent. The residual solvent signals were employed as internal standards. Elemental analysis data were obtained on a Perkin-Elmer CHN 2400.

Syntheses of Complexes. The novel complex $[Ir(Fppy)_2(dmb)]^+$, **Ir1**, was prepared and isolated as its PF_6^- salt by the well-established Nonoyama procedure,[15] with synthesis of the *μ*-chloro-bridged cyclometalated Ir(III) dimer as an intermediate, and followed by introduction of the *dmb* ligand.[13b,c,16] Complexes $[Ir(ppy)_2(NN)]^+$, *NN* = *dmb* (**Ir2**), *phen* (**Ir3**), and Ph_2phen (**Ir4**), were synthesized by a procedure similar to one reported in the literature.[8d,10f,12c,13,16,17] Chart 1 summarizes their chemical structures.

*$[Ir(Fppy)_2(dmb)][PF_6]$ (**Ir1**).* $IrCl_3·H_2O$ (Aldrich) (395 mg, 1.32 mmol) and *FppyH* (450 *μ*L, 3.01 mmol) were dissolved in a 5/3 (v/v) mixture of ethylene glycol monoethyl ether/water (20 mL) and heated at reflux with stirring for 15 h. After being cooled to room temperature, *dmb* (242 mg, 1.33 mmol) was added to the mixture, which was refluxed again for 22 h. Upon cooling, the mixture was washed with diethyl ether. The greenish yellow precipitate, obtained after slow addition of aqueous solution of ammonium hexafluorophosphate, was filtered and washed with water and recrystallized in dichloromethane/*n*-pentane. The solid was dried under vacuum to obtain 467 mg (0.52 mmol), 40% yield, of pure product. Anal. Calcd for $IrC_{34}H_{24}N_4F_{10}P$: C, 45.29%; H, 2.68%; N, 6.21%. Found: C, 45.51%; H, 2.68%; N, 6.17%. ^1H NMR (500 MHz, CD_2Cl_2) *δ*/ppm: 8.33 (m, 4H), 7.83 (m, 4H), 7.50 (dd, *J* = 5.8; 0.8 Hz, 2H), 7.29 (dd, *J* = 5.8, 0.8 Hz, 2H), 7.04 (ddd, *J* = 7.6, 5.8, 1.4 Hz, 2H), 6.59 (ddd, *J* = 12.5, 9.2, 2.4 Hz, 2H), 5.74 (dd, *J* = 8.3, 2.4 Hz, 2H), 1.53 (s, 6H).

Chart 1. List of Chemical Structures for Investigated Ir(III) Complexes and PEG-DMA550

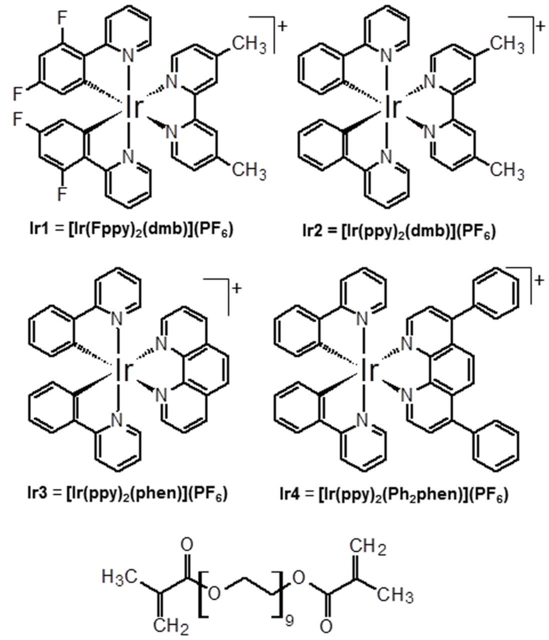

*$[Ir(ppy)_2(dmb)][PF_6]$ (**Ir2**).* $IrCl_3·H_2O$ (Aldrich) (230 mg, 0.77 mmol) and *ppyH* (245 *μ*L, 1.67 mmol) were heated at reflux for 8 h in ethylene glycol monoethyl ether (10 mL) and water (6 mL) to produce the *μ*-chloro-bridged cyclometalated Ir(III) precursor. After being cooled to room temperature, *dmb* (145 mg, 0.80 mmol) was added to the mixture and refluxed again for 20 h. After addition of NH_4PF_6, the yellow precipitate was filtered, washed, and recrystallized in dichloromethane/*n*-pentane, to obtain 420 mg (0.51 mmol), 65% yield, of pure product. Anal. Calcd for $IrC_{34}H_{28}N_4F_6P$: C, 49.21%; H, 3.40%; N, 6.75%. Found: C, 49.10%; H, 3.43%; N, 6.62%. ^1H NMR (200 MHz, CD_2Cl_2) *δ*/ppm: 8.29 (s, 2H), 7.95 (d, *J* = 7.7 Hz, 2H), 7.77 (m, 6H), 7.50 (d, *J* = 5.8 Hz, 2H), 7.23 (d, *J* = 5.5 Hz, 2H), 7.00 (m, 6H), 6.31 (d, *J* = 7.5 Hz, 2H), 1.55 (s, 6H).

*$[Ir(ppy)_2(phen)][PF_6]$ (**Ir3**).* $IrCl_3·H_2O$ (Aldrich) (190 mg, 0.63 mmol) and *ppyH* (205 *μ*L, 1.40 mmol) were heated at reflux for 8 h in ethylene glycol monoethyl ether (7.5 mL) and water (4.5 mL). Next, *phen* (120 mg, 0.67 mmol) was added to the mixture, which was heated at reflux again for 20 h. After precipitation with NH_4PF_6 and recrystallization in dichloromethane/*n*-pentane, 250 mg (0.29 mmol), 45% yield, of pure yellow product was obtained. Anal. Calcd for $IrC_{34}H_{24}N_4F_6P$: C, 49.45%; H, 2.93%; N, 6.78%. Found: C, 49.63%; H, 3.07%; N, 6.51%. ^1H NMR (200 MHz, CD_2Cl_2) *δ*/ppm: 8.66 (d, *J* = 8.0 Hz, 2H), 8.38 (d, *J* = 4.0 Hz, 2H), 8.24 (s, 2H), 7.75 (m, 10H), 7.35 (d, *J* = 5.2 Hz, 2H), 7.00 (m, 4H), 6.40 (d, *J* = 6.6 Hz, 2H).

*$[Ir(ppy)_2(Ph_2phen)][PF_6]$ (**Ir4**).* $IrCl_3·H_2O$ (Aldrich) (160 mg, 0.54 mmol) and *ppyH* (175 *μ*L, 1.20 mmol) were heated at reflux for 8 h in ethylene glycol monoethyl ether (7.5 mL) and water (4.5 mL). After being cooled to room temperature, Ph_2phen (440 mg, 1.32 mmol) was added to the mixture and refluxed again for 20 h, and the compound was precipitated as PF_6 salt and recrystallized in dichloromethane/*n*-pentane to obtain 240 mg (0.25 mmol), 47% yield, of pure orange-yellow product. Anal. Calcd for $IrC_{46}H_{32}N_4F_6P$: C, 56.49%; H, 3.30%; N, 5.73%. Found: C, 56.65%; H, 3.51%; N, 5.70%. ^1H NMR (200

dx.doi.org/10.1021/ic500070s | Inorg. Chem. 2014, 53, 4089−4099

MHz, $CDCl_3$) δ/ppm: 8.32 (d, J = 5.3 Hz, 2H), 8.18 (s, 2H), 7.94 (d, J = 8.1 Hz, 2H), 7.74 (m, 6H), 7.58 (m, 12H), 7.06 (m, 6H), 6.43 (d, J = 6.9 Hz, 2H).

PEG-DMA550 Film Preparation. Poly(ethyleneglycol)-dimethacrylate (PEG-DMA550) films, with nine ethylene-glycol spacers, Chart 1, containing Ir(III) complexes were prepared similarly to the procedure reported in the literature.[18] Complexes were dissolved in PEG-DMA550 fluids with 2,2′-azobis(2,4-dimethylvaleronitrile), DuPont, 1 wt %, as an initiator in 1.0 cm path length glass cuvettes, which were sealed with rubber septa and heated overnight at 50 °C under vacuum to yield optically transparent films. The concentration of Ir(III) complexes was kept within the range 25−35 μmol L^{-1}.

Photophysical Measurements. UV−vis absorption spectra were recorded on a Hewlett-Packard 8453 diode array spectrophotometer. Steady-state and time-resolved emission spectra were recorded on a ISS-PC1 photon-counting spectrofluorometer or an Edinburgh Instruments FLS920 time-correlated single photon counting emission spectrometer equipped with a Hamamatsu R928P photomultiplier tube (PMT). A xenon lamp (λ_{ex} = 365 nm, 4 nm bandwidth, with a 389 nm long pass filter) or an ISS laser (λ_{ex} = 378 nm, frequency = 20 kHz) were used with the ISS-PC1 as excitation light source for steady-state or time-resolved measurements, respectively. For experiments in the FLS920, a xenon lamp (λ_{ex} = 365 nm, 5 nm bandwidth, with a 395 nm long pass filter) or a pulsed Edinburgh Instruments EPLED-360 LED laser (λ_{ex} = 369 nm, frequency = 20 kHz) was employed. Emission intensity of steady-state spectra was corrected for system spectral response. For 298 K measurements, the absorbance of sample solutions in acetonitrile was set between 0.1 and 0.3 in a four polished face cuvette with 1.000 cm optical path length. Solutions were deoxygenated with argon for at least 10 min prior to measurement. For 77 K experiments, samples were prepared in a mixture of propionitrile/butyronitrile 4/5 (v/v) in cylindrical quartz tubes, 0.4 cm radius, and were inserted into a Dewar flask containing liquid N_2.

Emission quantum yields (ϕ) of complexes in acetonitrile at 298 K were measured applying the methodology earlier reported by Friend et al.[19] using an $BaSO_4$-coated integration sphere, model 1-M-2 (Edinburgh), with samples positioned at its center, as well as calculated from eq 1 using $[Ru(bpy)_3][PF_6]$ in the same solvent as the reference (λ_{ex} = 420 nm, 5 nm bandwidth, with a 435 nm long pass filter). The results of both techniques gave excellent agreement.

$$\phi_{Ir} = \phi_{ref} \frac{P_{Ir}}{P_{ref}} \frac{A_{ref}}{A_{Ir}} \tag{1}$$

where ϕ_{Ir} is the emission quantum yield of the sample; ϕ_{ref} is the emission quantum yield of the reference (0.095 in acetonitrile[20]); A_r is the absorbance of the sample at the excitation wavelength; A_{ref} is the absorbance of the reference at the excitation wavelength; P_{Ir} is the integral of the sample phosphorescence spectrum; and P_{ref} is the integral of the reference phosphorescence spectrum.

Theoretical Calculations. Electron density calculations for the series of complexes were conducted with Gaussian 09W software.[21] Optimization of ground-state structures was performed by using DFT with the B3LYP functional. The LanL2DZ[22a−c] and 6-31G(d,p)[22d,e] basis sets were used to treat iridium and all other atoms, respectively. TD-DFT calculations were then performed to estimate energies and oscillator strengths of the lowest energy ten singlet and five triplet transitions for all complexes. Calculations were carried out in acetonitrile as solvent by using a Polarizable Continuum Model (PCM). Electron density populations were plotted using GaussView 5.0.[23]

Franck−Condon Analyses for Emission Spectra. Franck−Condon band shape analysis for emission spectrum provides information about contributing vibrational modes and structural changes between the emitting excited state and the ground state.[12d,14a,24] In the versions in eq 2 or 3, one or two vibrational acceptor mode(s), respectively, are included. They are averages of the multiple modes coupled to the transition between the emitting excited state and the ground state. Contributions from low-frequency modes and the solvent are treated classically and included in the band widths of individual vibronic transitions. Prior to the spectral fitting analysis, the number of photons at a given wavelength were corrected to the wavenumber scale by using the relationship, $I(\tilde{\nu}) = I(\lambda) \times \lambda^2$.[25]

$$I(\tilde{\nu}) = \sum_{\nu_M=0}^{\infty} \left(\frac{E_0 - \nu_M \hbar\omega_M}{E_0}\right)^3 \left(\frac{S_M^{\nu_M}}{\nu_M!}\right) \exp\left[-4 \ln 2 \left(\frac{\tilde{\nu} - E_0 + \nu_M \hbar\omega_M}{\tilde{\nu}_{1/2}}\right)^2\right] \tag{2}$$

$$I(\tilde{\nu}) = \sum_{\nu_M=0}^{\infty} \sum_{\nu_L=0}^{\infty} \left(\frac{E_0 - \nu_M \hbar\omega_M - \nu_L \hbar\omega_L}{E_0}\right)^4 \left(\frac{S_M^{\nu_M}}{\nu_M!}\right)\left(\frac{S_L^{\nu_L}}{\nu_L!}\right) \times \exp\left[-4 \ln 2 \left(\frac{\tilde{\nu} - E_0 + \nu_M \hbar\omega_M + \nu_L \hbar\omega_L}{\tilde{\nu}_{1/2}}\right)^2\right] \tag{3}$$

In these equations, $I(\tilde{\nu})$ is the emission intensity at the energy $\tilde{\nu}$ (cm^{-1}). E_0 is the energy gap between the zeroth vibrational levels in the ground and excited states. $\hbar\omega_M$ and $\hbar\omega_L$ are the quantum spacings for averaged medium- and low-frequency vibrational modes, respectively.[12d] S_M and S_L are the associated electron-vibrational coupling constants or Huang−Rhys factors,[26] related to structural differences between excited and ground states along the displacement normal coordinates of the coupled average medium- and low-frequency vibrational modes, respectively. $\tilde{\nu}_{1/2}$ is the full width at half-maximum (fwhm) for an individual vibronic line.[27]

In the fitting procedure, E_0, $\hbar\omega$, S, and $\tilde{\nu}_{1/2}$ were optimized with a least-squares minimization routine with application of a Generalized Reduced Gradient (GRG2) algorithm.[28] The summation was carried out from ν^* = 0 in the excited state to levels ν = 0→10 in the ground state.

RESULTS AND DISCUSSION

Absorption Spectra. Absorption spectra of complexes **Ir1** and **Ir2**, Figure 1, exhibit an intense band around 255 nm with high molar extinction coefficients ($\varepsilon \approx 5 \times 10^4$ L mol^{-1} cm^{-1}) arising from a $\pi\pi^*$ transition at the ancillary *dmb* ligand (i.e., ligand centered, LC_{dmb}). Intense bands at 260 and 270 nm for **Ir3** and **Ir4** can be assigned to LC_{phen} and $LC_{ph2phen}$ transitions, respectively. *Xppy* $\pi\pi^*$ states are expected to appear at higher energies than for the ancillary NN ligands due to their

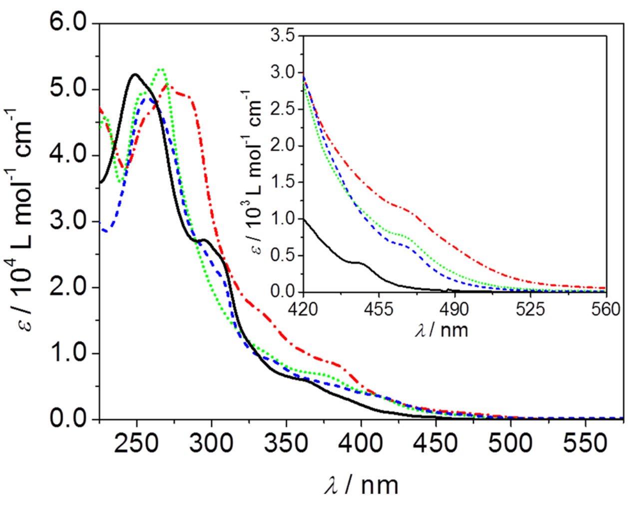

Figure 1. Absorption spectra of complexes **Ir1** (black —), **Ir2** (blue – – –), **Ir3** (green ···), and **Ir4** (red – · – ·) in acetonitrile with an enhanced scale shown in the inset.

destabilization upon cyclometalation with Ir(III).[29] In the lower-energy region (λ > 280 nm), absorption spectra are featureless with an overlap of transitions ascribed to mixed spin character excited states due to strong spin−orbit coupling effect,[9] with ξ_{Ir} = 4430 cm^{-1}.[30] However, bands from 320 to 440 nm can be assigned to largely spin-allowed metal-to-ligand charge-transfer (MLCT) transitions, with ε values in the range $(2 - 10) \times 10^3$ L mol^{-1} cm^{-1}. The lowest-lying absorption from 440 to 480 nm ($\varepsilon \approx 0.8 \times 10^3$ L mol^{-1} cm^{-1}) is tentatively ascribed to the lowest-lying spin-forbidden transition, T_1, assumed to be the lowest ^{3}MLCT state. The relatively high intensity for this nominally spin-forbidden transition is due to spin−orbit coupling, which also facilitates intersystem crossing between nominally singlet and triplet states. Furthermore, Ir(III) dd transitions are typically at much higher energies.[5c]

In addition, although not observable in absorption spectra, there is experimental evidence (τ, k_{nr} and k_r, and spectral feature changes with rigidity and temperature (T)) for an energetically close-lying, ligand-based $\pi\pi^*$ excited state, ^{3}LC.[1c,i] As suggested in Scheme 1, it is presumably mixed with the

Scheme 1. Orbital Description of the Lowest Excited State, T_1, Illustrating Mixing between ^{3}MLCT(1) and ^{3}LC, for a > b

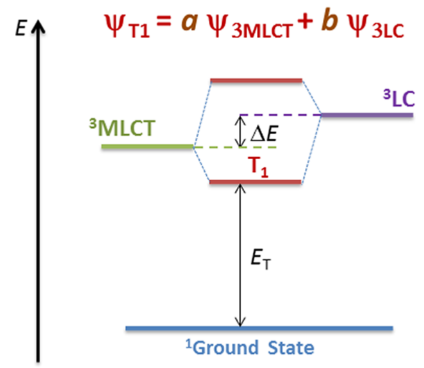

lowest-lying ^{3}MLCT(1) state resulting in mixed orbital character for the lowest excited state, T_1, with $\Psi_{T1} = a\Psi_{3MLCT} + b\Psi_{3LC}$ as the wave function description.[1c,i] The contribution of each individual state in T_1 is given by a and b, respectively, for ^{3}MLCT and ^{3}LC. In the diagram, emission from complexes occurs at E_T and ΔE is the zero order energy difference between the unmixed states ^{3}MLCT and ^{3}LC. Orbitally, the MLCT and LC excited states share a common π^* acceptor with the hole in either the lowest dπ orbital on the metal or a π orbital on a ligand with the excited-state configurations, $d\pi^5\pi^{*1}$ for ^{3}MLCT(1) and $\pi^1\pi^{*1}$ for ^{3}LC. The orbital origin of the mixing between states in T_1 is through $d\pi^5-\pi$ mixing with partial oxidation of the ligands by electron donation to the metal induced by the electronic effect on the dπ levels of the diimine ligand.

Emission Spectra and Photophysical Properties at 298 K. Emission spectra for the Ir(III) complexes in acetonitrile at 298 K, Figure 2A, are broad and structureless, independent of the excitation wavelength consistent with MLCT emission, with T_1 more influenced by the lowest MLCT triplet, ^{3}MLCT(1).[1i,31] Emission parameters are summarized in Table 1. Emission maxima vary with the nature of the substituents with emission from **Ir1** (λ = 522 nm) blue-shifted relative to the other three due to the presence of

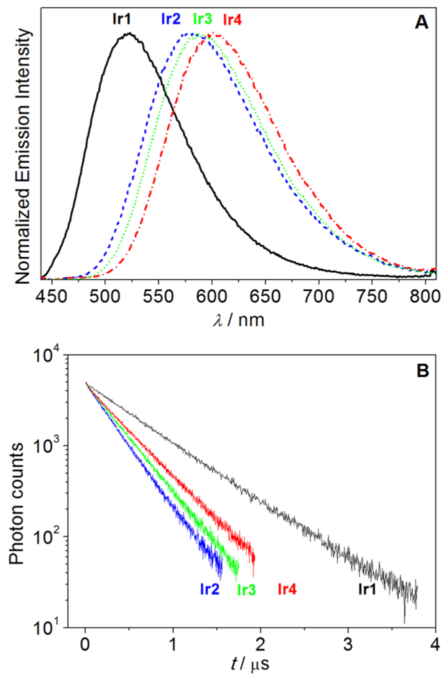

Figure 2. Emission spectra (A) and decay profiles (B) for complexes **Ir1** (black), **Ir2** (blue), **Ir3** (green), and **Ir4** (red) in acetonitrile at 298 K.

Table 1. Excited-State Parameters of the Investigated Complexes in Acetonitrile at 298 K

complex	λ/nm	ϕ	$\tau/\mu s$	$k_r/10^5$ s^{-1}	$k_{nr}/10^5$ s^{-1}
Ir1	522	0.96 ± 0.10	0.66 ± 0.03	15 ± 2	0.6 ± 0.1
Ir2	580	0.23 ± 0.02	0.31 ± 0.02	7.4 ± 0.8	25 ± 3
Ir3	590	0.27 ± 0.03	0.36 ± 0.02	7.5 ± 0.8	20 ± 2
Ir4	602	0.29 ± 0.03	0.43 ± 0.02	6.7 ± 0.7	17 ± 2

stabilizing electron-withdrawing fluoro groups in the cyclometalated ppy ligand framework. A red-shift of the emission is observed with an increase in the electron-withdrawing ability of the substituents on the diimine ligands. These qualitative trends are consistent with the results of the TD-DFT calculations summarized in the following section.

Remarkably, the emission quantum yield for **Ir1** is ∼1, which makes it distinctive as the most strongly emissive complex in the heteroleptic $[Ir(Xppy)_2(NN)]^+$ series. Its emission lifetime (τ = 0.66 μs) is relatively short despite the high emission efficiency as observed for other Ir(III) complexes.[1i] Complex **Ir4** exhibits a longer emission lifetime (τ = 0.43 μs) than those for **Ir3** (τ = 0.36 μs) and **Ir2** (τ = 0.31 μs) with emission quantum yields of 0.29, 0.27, and 0.23, respectively. The relatively short "triplet" lifetimes for all complexes arise from spin−orbit coupling-induced mixing of singlet spin character into the excited state, which, in turn, enhances mixing with the ground state. For practical applications, these are suitable photophysical characteristics for light-emitting devices, for which τ should be short enough to allow rapid repopulation of the emitting excited state with ϕ at least 0.20 for sufficient light output, and **Ir2** was recently applied for the first time in the active layer of a LEC.[13]

The quantities ϕ and τ are related to the rate constants for radiative (k_r) and nonradiative (k_{nr}) excited-state decay as shown in eqs 4a and 4b. From its quantum yield, decay of **Ir1** excited state is dominated by k_r. For excited states with similar

dx.doi.org/10.1021/ic500070s | Inorg. Chem. 2014, 53, 4089−4099

Table 2. Calculated Energies and Oscillator Strengths for Lowest-Energy Singlet (S_1) and Triplet (T_1) Transitions

complex	excited state	transition	energy (wavelength)	oscillator strength
Ir1	S_1	HOMO→LUMO	2.863 eV (433 nm)	0.0002
	T_1	HOMO→LUMO (85%)	2.826 eV (439 nm)	
		HOMO−6→LUMO (15%)		
Ir2	S_1	HOMO→LUMO	2.608 eV (475 nm)	0.0002
	T_1	HOMO→LUMO	2.581 eV (480 nm)	
Ir3	S_1	HOMO→LUMO	2.577 eV (481 nm)	0.0003
	T_1	HOMO→LUMO	2.547 eV (487 nm)	
Ir4	S_1	HOMO→LUMO	2.545 eV (487 nm)	0.0004
	T_1	HOMO→LUMO	2.511 eV (494 nm)	

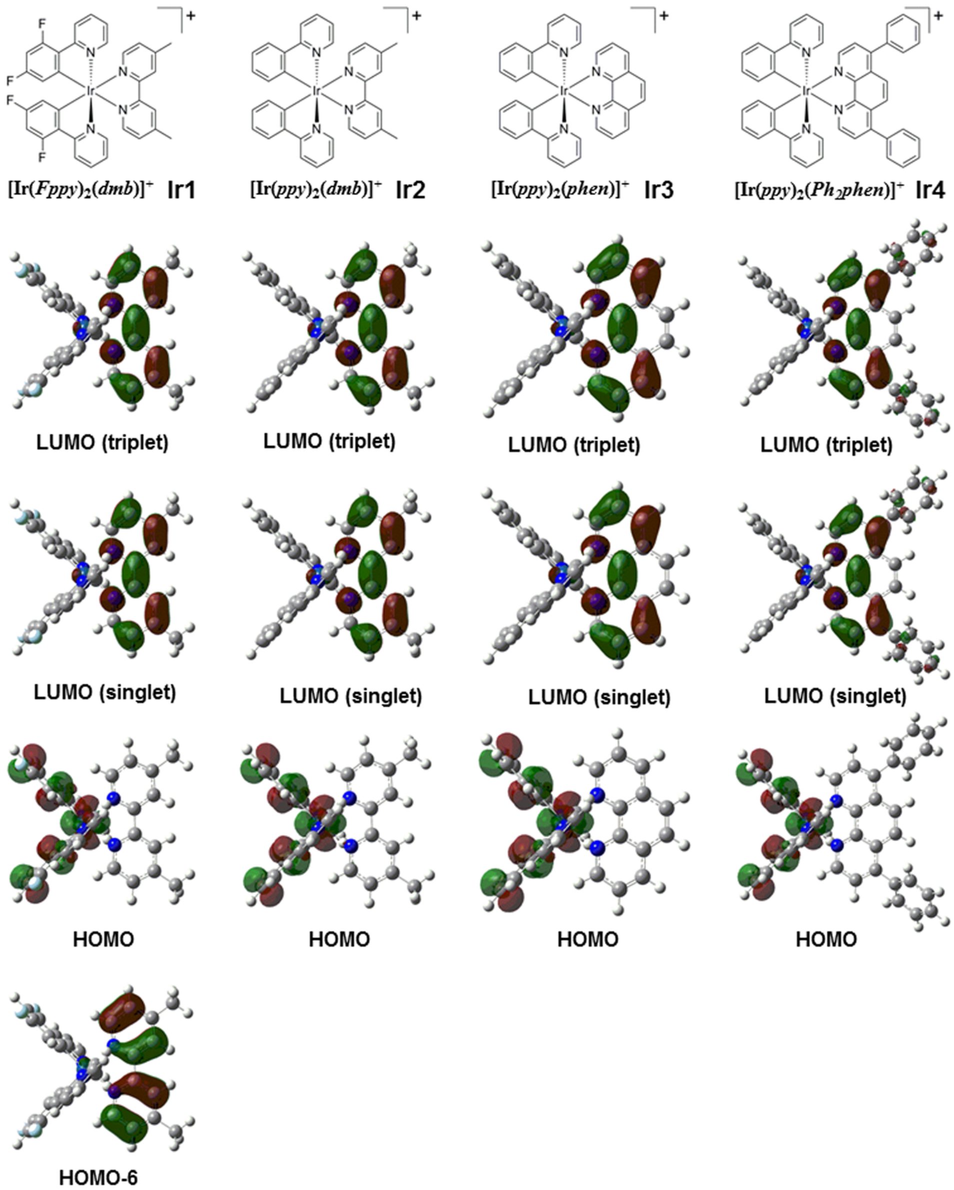

Figure 3. Chemical structures and molecular orbital contours for the main molecular orbitals of investigated Ir(III) complexes.

character, k_r varies as the square of the transition dipole moment, $\vec{\mu}$, and the cube of the average emission energy, $\sim E_T{}^3$: $k_r \propto \vec{\mu}^2 E_T^3$.[1i,12d] k_r is also closely related to the spin−orbit coupling of the emissive excited state, which comes from a mathematical formalism that relates k_r to the inverse of the energy difference between two perturbing excited states ($k_r \propto -\Delta E$), for example, ^{3}MLCT and ^{3}LC.[1i] The enhanced value of k_r for complex **Ir1** ($15 \times 10^5\ s^{-1}$) relative to $k_r \approx 7.4 \times 10^5\ s^{-1}$ for the other three complexes is remarkable. Although the electronic origin of the effect is not obvious, an experimentally grounded explanation for the twice higher k_r is a distinct excited-state character for the **Ir1** complex, with pronounced mixing between ^{3}MLCT and ^{3}LC states as depicted in Scheme 1, differing from the pure ^{3}MLCT emission for the other three

Table 3. Electron Density Populations of Molecular Orbitals Defining S_1 and Emissive T_1 States for Complexes Ir1−Ir4

	Ir1			Ir2			Ir3			Ir4		
orbital	iridium	*Fppy*	*dmb*	iridium	*ppy*	*dmb*	iridium	*ppy*	*phen*	iridium	*ppy*	*Ph$_2$phen*
$LUMO_{(triplet)}$	3.41	2.98	**93.61**	3.30	2.47	**94.23**	3.81	2.55	**93.64**	3.74	2.34	**93.92**
$LUMO_{(singlet)}$	3.29	2.26	**94.45**	3.31	2.22	**94.47**	3.89	2.48	**93.63**	3.94	2.30	**93.76**
HOMO	**46.09**	**50.71**	3.20	**47.71**	**48.67**	3.62	**47.10**	**49.25**	3.65	**47.15**	**48.99**	3.86
HOMO−6	2.26	1.72	**96.02**									

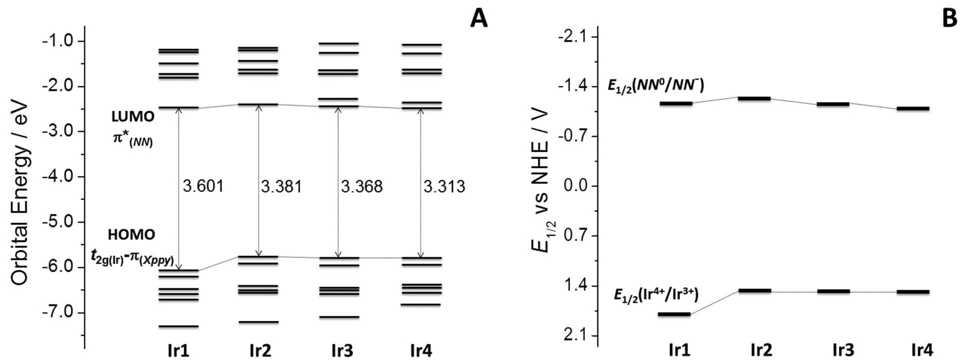

Figure 4. (A) Orbital energies calculated by B3LYP/LanL2DZ (Ir) and B3LYP/6-31(d,p) (CHNF) and (B) redox potentials for the series **Ir1−Ir4**, from cyclic voltammetry measurements; see Figure S3 in the Supporting Information.

complexes. Variations in k_{nr} in the series are discussed in a later section.

$$\phi = \frac{k_r}{k_r + k_{nr}} \tag{4a}$$

$$\tau = \frac{1}{k_r + k_{nr}} \tag{4b}$$

Time-Dependent Density Functional Theory Calculations. Relevant energies and oscillator strengths for the lowest-energy singlet (S_1) and triplet (T_1) transitions are summarized in Table 2. The results of calculations on the first ten singlet and five triplet transitions are also listed in the Supporting Information, Tables S2−S5. As shown in Supporting Information Figure S2, calculated energies and oscillator strengths for the singlet transitions agreed very well with experimental absorption spectra for all four complexes.

As shown in Table 2, the lowest-energy spin-allowed transitions for all four complexes to give S_1 are HOMO → LUMO transitions. From Figure 3 and Table 3, the HOMO is largely $d\pi_{Ir}$ mixed with the π_{Xppy}, and the LUMO is largely a π^* orbital on the diimine ligand, with S_1 mainly MLCT in character with a minor contribution of a ligand-to-ligand charge-transfer (LLCT) transition. For convenience, in further discussions this excited state is referred to as $^1MLCT_{Ir(ppy)\rightarrow NN}$. As shown in Figure 4A, LUMO energies decrease through the series from **Ir2** to **Ir4** due to the enhanced increasing electron-withdrawing capability of the *NN* ligand. A significant change in the HOMO energy for **Ir1** is observed due to the electron-withdrawing F substituents on the *ppy* ligand.

Variations in calculated S_1 energies are also in good agreement with relative redox potentials in acetonitrile, Table 4 and Figure 4B. Complexes **Ir2−Ir4** exhibit a reversible one-electron oxidation at ∼1.48 V vs NHE, presumably from the expected Ir^{4+}/Ir^{3+} couple, which shifts anodically for complex **Ir1** with the oxidation appearing at 1.80 V. Reversible, ligand-based reduction appears at −1.22, −1.14, and −1.09 V for complexes **Ir2**, **Ir3**, and **Ir4**, respectively. These values show

Table 4. Redox Potentials for Metal-Based Oxidation (Ir^{4+}/Ir^{3+}) and Ligand-Based Reduction (NN^0/NN^-) versus NHE in Acetonitrile, ∼0.5 mmol L^{-1}, at Room Temperature from Cyclic Voltammetry Measurements[a]

complex	$E_{1/2}(NN^0/NN^-)$/V	$E_{1/2}(Ir^{4+}/Ir^{3+})$/V
Ir1	−1.15	1.80
Ir2	−1.22	1.47
Ir3	−1.14	1.48
Ir4	−1.09	1.49

[a]Figure S3 in the Supporting Information.

that changes in the HOMO caused by substituent changes in the *ppy* framework influence oxidation of Ir(III) complexes, while variations in the LUMO are dictated by the diimine acceptor ligand.

The next two lowest-lying singlet excited states (S_2 and S_3, respectively) are ascribed to HOMO → LUMO+1 and HOMO → LUMO+2 transitions, Tables S2−S6 in the Supporting Information. They are mainly related to *ppy* MLCT and IL for **Ir1** and **Ir2**, with the electron density in both LUMO+1 and LUMO+2 residing significantly on the cyclo- metalating ppy ligands. For **Ir3** and **Ir4**, LUMO+1 is largely π^*NN and S2 is an $^1MLCT_{Ir(ppy)\rightarrow NN}$ state, while S3 is related to a ppy MLCT/IL transition with LUMO+2 mainly π^*_{Xppy}. TDDFT results diverge for the four complexes after the fourth lowest-lying singlet excited state (S_4), with transitions ascribed to MLCT/LLCT, from both Ir(III) and *ppy* to the *NN* ligand, or intraligand *ppy* excited states.

In the calculations, the triplet T_1 states for complexes **Ir2−Ir4** follow the same trend of S_1, arising from formally spin-forbidden MLCT transitions, which gain allowedness through spin−orbit coupling. They are lowest-lying and are the origin of the observed emissions. However, exclusively for **Ir1**, the T_1 transition is 15% HOMO−6, localized in the π orbital of the *dmb* ligand, and, therefore, based on the calculations, T_1 for **Ir1** is of mixed $^3MLCT_{Ir(ppy)\rightarrow NN}/^3LC_{NN}$ character, with a = 0.85 and b = 0.15.

dx.doi.org/10.1021/ic500070s | Inorg. Chem. 2014, 53, 4089−4099

Emission Spectral Fitting at Room Temperature. Results and Applications. Franck–Condon analyses for emission spectra at room temperature in acetonitrile were conducted by application of the single average mode approximation and eq 2. Experimental spectra are compared to calculated ones in Figure 5. The agreement between experimental and calculated spectra was excellent with high correlation coefficients in all cases, with $R^2 \geq 0.9998$. Spectral fitting parameters obtained from the fits (E_0, S, and $\hbar\omega_M$) are listed in Table 5.

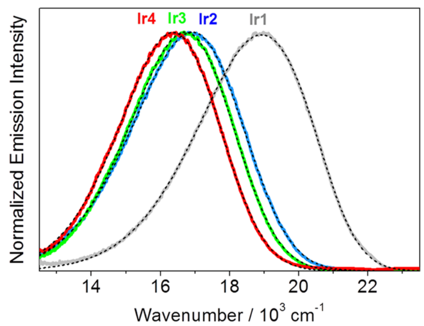

Figure 5. Experimental (colored solid curves) and simulated emission spectra (black broken curves) by use of eq 2 with the parameters listed in Table 5 in acetonitrile at 298 K.

Table 5. Emission Spectral Fitting Parameters in Acetonitrile at 298 K

complex	E_0/cm^{-1}	$\tilde{\nu}_{1/2}$/cm^{-1}	$\hbar\omega_M$/cm^{-1}	S_M	$\ln[FC_{(calc)}]$
Ir1	19 920	2350	1380	1.34	−21.31
Ir2	17 570	2810	1390	0.93	−20.33
Ir3	17 230	2740	1380	0.79	−21.66
Ir4	16 820	2730	1340	0.71	−22.61

As shown in Figure 6, E_0 values in Table 5 are proportional to the difference in redox potentials between oxidation, $E_{1/2}(Ir^{4+}/Ir^{3+})$, and reduction, $E_{1/2}(NN^0/NN^-)$, a characteristic feature of MLCT excited states.[32] The observed linear slope is less than unity, around 0.82, because emission energy includes losses by intersystem crossing and contributions from outer- and inner-sphere reorganization energies. Similar deviations were also reported for series of MLCT emitters, Re(I), Ru(II), and Os(II) complexes.[32]

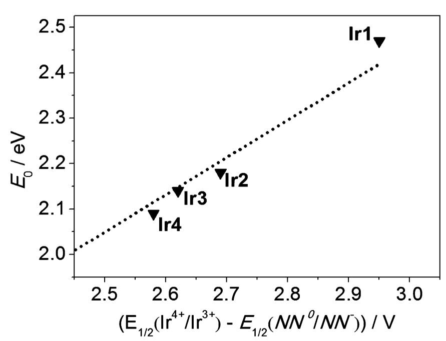

Figure 6. Plot of E_0 from emission spectral fitting vs ($E_{1/2}(Ir^{4+}/Ir^{3+}) - E_{1/2}(NN^0/NN^-)$) in acetonitrile at room temperature.

According to Table 5, the magnitude of the quantum spacing for the average acceptor mode, $\hbar\omega_M$, is ~1370 cm^{-1}, consistent with an average of a series of C–C/C–N stretching modes in the *NN* acceptor ligands[33] and with results obtained earlier for related MLCT $d\pi^6$ polypyridyl emitters.[14b,24a] The electron-vibrational coupling constant or Huang–Rhys factor, S_M, is a measure of the extent of the skeletal structural change in the acceptor ligand and increases with energy gap, E_0, as found earlier for MLCT excited states of Os(II)[34] and Re(I) polypyridyl complexes.[32c] Therefore, FC analysis supports aforementioned discussions that T_1 character is largely $^3MLCT_{Ir(ppy)\to NN}$ at 298 K.

In the limit of applicability of the single mode approximation and in the weak vibrational coupling limit, with $E_0 \gg S_M\hbar\omega_M$ and $\hbar\omega_M \gg k_BT$, the rate constant for nonradiative decay is given by eq 5. In eq 5, the Franck–Condon weighted density of states, $\ln[FC_{(calc)}]$, can be calculated by using the parameters from emission spectral fitting and eqs 6 and 7.[12d,34]

$$\ln k_{nr} = \ln \beta_0 + \ln[FC_{(calc)}] \tag{5}$$

$$\ln[FC_{(calc)}] = -\frac{1}{2}\ln\left[\frac{\hbar\omega_M E_0}{(1000\ \text{cm}^{-1})^2}\right] - S_M - \frac{\gamma_0 E_0}{\hbar\omega_M} + \frac{(\gamma_0+1)^2\left(\frac{\Delta\tilde{\nu}_{0,1/2}}{\hbar\omega_M}\right)^2}{16\ln 2} \tag{6}$$

$$\gamma_0 = \ln\left(\frac{E_0}{S_M\hbar\omega_M}\right) - 1 \tag{7}$$

$$\beta_0 = \frac{\sqrt{2\pi}}{\hbar}\frac{V_k{}^2}{(1000\ \text{cm}^{-1})} \tag{8}$$

The quantity β_0 includes the vibrationally induced electronic coupling matrix element, V_k, which mixes the initial and final electronic states, eq 8. Calculated $\ln[FC_{(calc)}]$ values are listed in Table 5, and a plot of $\ln k_{nr}$ versus $\ln[FC_{(calc)}]$ is shown in Figure 7.

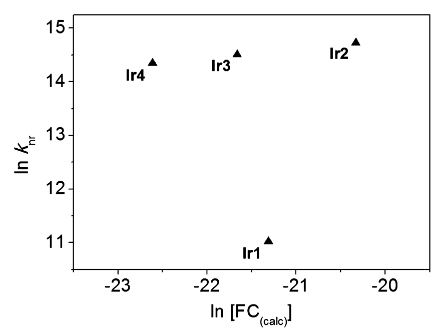

Figure 7. Plot of $\ln k_{nr}$ versus $\ln[FC_{(calc)}]$ from the k_{nr} values in Table 1 and the results of emission spectral fitting in Table 5 in acetonitrile at room temperature.

For complexes **Ir2**–**Ir4**, $\ln k_{nr}$ increases with $\ln[FC_{(calc)}]$, as predicted by eq 5 consistent with decay from emissive T_1 states with common $^3MLCT_{Ir(ppy)\to NN}$ origins. For these complexes, the commonly observed energy gap law relationship $\ln k_{nr} \propto -E_{em}$ is not observed, and the more complete expression in eq 5 is required to reconcile the data because of the differences in acceptor ligand through the series, with a different mix of ring skeletal vibrations.

Given the high emission efficiency, k_{nr} for complex **Ir1** is not known accurately but, nonetheless, deviates markedly from the trend shown by the other three. An additional difference in the series appears in the ~400 cm^{-1} decrease in bandwidth at half height, $\tilde{\nu}_{1/2}$, for **Ir1**, which, in the classical harmonic oscillator limit, is related by eq 9 to the solvent reorganization energy including low frequency modes treated classically, $(\lambda_{o,L})^{1/2}$.[12d] The decrease in bandwidth is symptomatic of a decrease in the extent of charge-transfer character in the emitting excited state, consistent with its mixed MLCT/LC character.

$$\tilde{\nu}_{1/2} = (16 k_B T \lambda_{o,L} \ln 2)^{1/2} \tag{9}$$

Emission Spectra at 77 K and Franck–Condon Analyses. A characteristic feature of MLCT emission from polypyridyl excited states is their sensitivity to medium.[35] A pronounced rigid medium effect, "rigidochromic effect",[1a,d,35a,b,36] exists between fluid and rigid media arising from the inability of the surrounding medium dipoles to reorient to change in dipole character between excited and ground states. A temperature dependence arises in bandwidth as described in eq 9 and band energy due to frequency changes in medium librations.[12d] By contrast, ligand-centered $\pi\pi^*$ excited states are relatively unaffected.

Emission spectra of the series **Ir1**–**Ir4** at 77 K in propionitrile/butyronitrile (4/5, v/v) are shown in Figure 8.

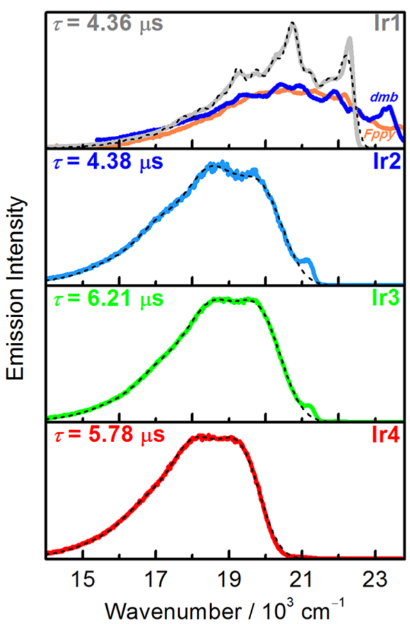

Figure 8. Experimental spectra (colored solid curves) and emission lifetimes in propionitrile/butyronitrile (4/5, v/v) at 77 K. Black broken curves represent simulated spectra of investigated complexes by using eq 3 or 10 with the parameters listed in Table 6. Simulated spectra of *dmb* and *Fppy* are shown in Figure S4 in the Supporting Information.

In the frozen medium, band energy blue-shifts of ~2700 cm^{-1} occur compared to room temperature in acetonitrile, consistent with their MLCT character. These emissions are notably intense with $\phi \approx 1$ and for **Ir2**–**Ir4** are relatively broad with similar band shapes. By contrast, emission from **Ir1** is narrow and highly structured and similar in band shape to emission from the free dmb ligand at 77 K, Figure 8, with a ligand-centered $\pi\pi^*$ origin.[29] Emission lifetimes at 77 K are in the 4.35–6.21 μs range as shown in Figure 8 and much longer than those at room temperature.

The results of multimode Franck–Condon analyses of the spectra are summarized in Table 6 with fits compared to experimental spectra in Figure 8. Spectra for complexes **Ir2**–**Ir4** were adequately reproduced ($R^2 \geq 0.9934$) by including both low-frequency ($\hbar\omega_L$) and medium-frequency averaged vibrational modes ($\hbar\omega_M$), eq 3. For these complexes, the values of $\hbar\omega_M$ and $\hbar\omega_L$ derived from the fits are ~1380 and ~410 cm^{-1}, consistent with earlier results of MLCT emission,[14b,24a] and arise from acceptor ligand skeletal modes and low frequency Ir–N stretching modes, respectively. These properties and the decrease in $\tilde{\nu}_{1/2}$ from ~2750 to ~1200 cm^{-1} upon cooling are both consistent with emitting T_1 excited states for **Ir2**–**Ir4** at 77 K that are mainly MLCT$_{Ir(ppy)\rightarrow NN}$ in character, although with some extent of ^{3}LC$_{NN}$ contribution.

Two-mode fitting could not satisfactorily reproduce the narrow, structured 77 K spectrum of **Ir1**. Although the simulation is not enough yet, better agreement was obtained with a three-mode analysis including a medium-low-frequency vibrational mode ($\hbar\omega_{ML}$), eq 10. In the three-mode analysis, the summation was carried out from $v^* = 0$ in the excited state to levels $v = 0 \rightarrow 5$ in the ground state.

$$I(\tilde{\nu}) = \sum_{\nu_M=0}^{\infty} \sum_{\nu_{ML}=0}^{\infty} \sum_{\nu_L=0}^{\infty} \left(\frac{E_0 - \nu_M \hbar\omega_M - \nu_{ML}\hbar\omega_{ML} - \nu_L \hbar\omega_L}{E_0} \right)^4 \times \left(\frac{S_M{}^{\nu_M}}{\nu_M!} \right) \left(\frac{S_{ML}{}^{\nu_{ML}}}{\nu_{ML}!} \right) \left(\frac{S_L{}^{\nu_L}}{\nu_L!} \right) \times \exp\left[-4 \ln 2 \left(\frac{\tilde{\nu} - E_0 + \nu_M \hbar\omega_M + \nu_{ML}\hbar\omega_{ML} + \nu_L \hbar\omega_L}{\tilde{\nu}_{1/2}} \right)^2 \right] \tag{10}$$

Emission spectra of *dmb* and *Fppy* at 77 K were also fitted to eq 10 with optimized parameters summarized in Table 6. The $\tilde{\nu}_{1/2}$ and $\hbar\omega$ values for **Ir1** and *dmb* are more comparable than those of *Fppy*, although even more satisfactory fits for dmb could have been obtained with a five-mode analysis.

In contrast to **Ir2**–**Ir4**, the low-temperature spectrum of **Ir1** is clearly indicative of emission from a lowest-lying T_1 state that is mainly triplet $\pi\pi^*$(*dmb*) in character, ^{3}LC$_{NN}$, with a relatively small extent of MLCT contribution (Figure S5 in the Supporting Information). Despite possessing $\pi\pi^*$ character, the Huang–Rhys factor for **Ir1** is smaller than for the free *dmb* ligand due to coordination to the metal and its influence on ligand rigidity. Comparison with the room-temperature data shows that an inversion in excited-state ordering occurs between room temperature, with emission from ^{3}MLCT$_{Ir(ppy)\rightarrow NN}$, and 77 K, with emission from ^{3}LC$_{NN}$ lowest-lying. Related observations have been made for high-energy MLCT state Re(I) polypyridyl-based emitters, where temperature-dependent inversion of MLCT and ligand-based $\pi\pi^*$ states is observed.[37]

The four complexes were also immobilized in PEG-DMA550 films, which are semirigid and optically transparent at room temperature. The emission spectra of the complexes in PEG-DMA550 fluid and film, before and after polymerization, are shown in Figure 9.

Emission in PEG-DMA550 fluid at 298 K is broad and structureless for all of the complexes, including **Ir1**, similar to fluid acetonitrile at 298 K, while polymerization and film formation result in only slight blue shifts ($\Delta\lambda \approx 16$ nm; $\Delta\tilde{\nu} \approx 520$ cm^{-1}). In even more rigid PEG-DMA550 films at 77 K,

Table 6. Spectral Fitting Parameters for Ir1−Ir4 and for *Fppy* and *dmb* in Propionitrile/Butyronitrile (4/5, v/v) at 77 K

	E_0/cm^{-1}	$\tilde{\nu}_{1/2}$/cm^{-1}	$\hbar\omega_M$/cm^{-1}	S_M	$\hbar\omega_{ML}$/cm^{-1}	S_{ML}	$\hbar\omega_L$/cm^{-1}	S_L
Fppy	23 790	570	1480	1.76	850	1.79	286	1.08
dmb	23 400	570	1520	1.81	980	1.21	530	0.58
Ir1	22 220	480	1500	1.22	980	0.61	490	0.76
Ir2	20 160	1260	1420	1.36			410	1.18
Ir3	20 090	1280	1380	1.18			400	1.11
Ir4	19 610	1110	1340	1.13			410	1.35

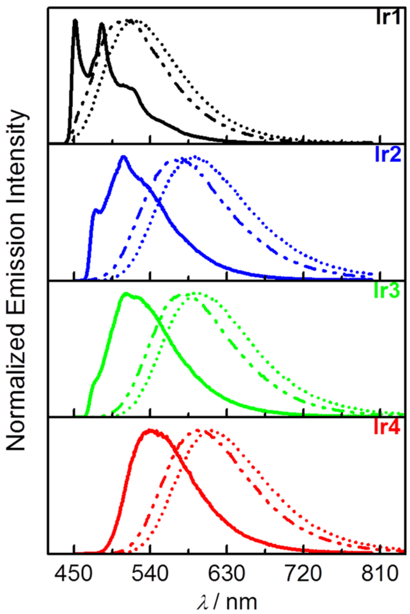

Figure 9. Emission spectra in PEG-DMA500 fluid at 298 K (····) and in PEG-DMA500 films at 298 K (−··−··) and 77 K (−).

emission is structured with profiles similar to those observed in propionitrile/butyronitrile (4/5, v/v) glass at 77 K. As in the nitrile glass, for **Ir1**, the change in emission with temperature in the film is consistent with the ^{3}MLCT$_{Ir(ppy)\rightarrow NN}$ to ^{3}LC$_{NN}$ inversion observed in the nitrile glass at 77 K. These results are consistent with important roles from both temperature and rigidity in the inversion between states, which is illustrated in Scheme 2.

Scheme 2 illustrates two elements of importance in describing excited-state structure in the series **Ir1−Ir4**. The excited-state properties of complexes **Ir2−Ir4** are dominated by low-lying T_1 states that can best be described as MLCT in character with broad, structureless emissions. The properties of these complexes vary systematically with emission energies and are systematically tunable by ligand changes. Nonradiative decay is satisfactorily accounted for by a quantitative version of the energy gap law parametrized by the results of emission spectral fitting, which includes variations in the acceptor ligand. Emission at 298 K originates from states largely ^{3}MLCT$_{Ir(ppy)\rightarrow NN}$ in character with little mixing with low-lying ^{3}LC$_{NN}$ states (orbital coefficients in Scheme 2 are $a \approx 1$, $b \approx 0$). At 77 K, the impact of the rigid medium effect on ^{3}MLCT$_{Ir(ppy)\rightarrow NN}$ increases MLCT excited-state energies, decreasing the gap to the lowest-lying ^{3}LC$_{NN}$ states, presumably with enhanced mixing with the lower-lying $\pi\pi^*$ ^{3}LC$_{NN}$ states.

For **Ir1**, the lowest-lying state at room temperature is also MLCT in character but with evidence for significant mixing between MLCT and low-lying LC states with a = 0.85, >b = 0.15 in the wave function in Scheme 2. Evidence for mixing

Scheme 2. Illustration of Excited-State Inversion for T_1 in Ir1 in the Temperature Decrease from 298 to 77 K

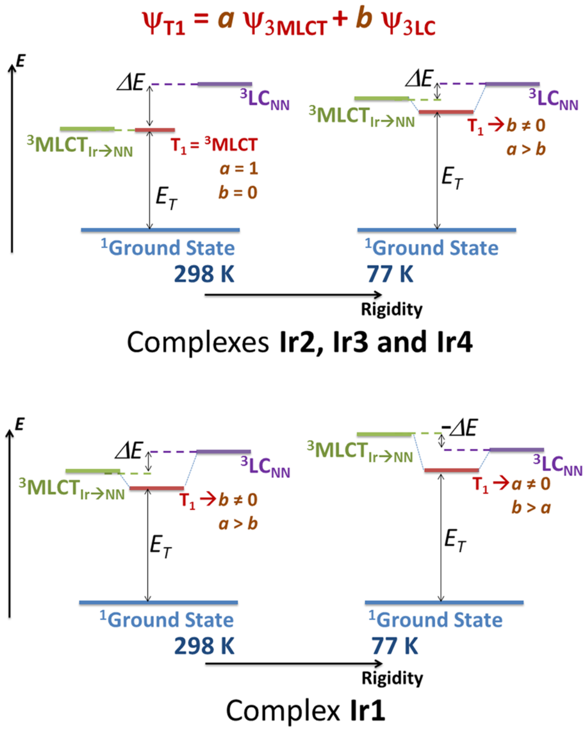

comes from the high emission quantum yield, greatly decreased magnitude for k_{nr}, and decreased magnitude of λ_o, the latter consistent with diminished charge-transfer character in the excited state. For this complex, cooling to 77 K results in an inversion in excited-state order with ^{3}MLCT$_{Ir(ppy)\rightarrow NN}$ > ^{3}LC$_{NN}$ as evidenced by the highly structured emission.

■ CONCLUSIONS

Quantitative evaluation of spectra, along with TD-DFT calculations, provided information about the extent of coupling between ^{3}MLCT$_{Ir(ppy)\rightarrow NN}$ and ^{3}LC$_{NN}$ states of a series of heteroleptic Ir(III) complexes, including the novel [Ir-(*Fppy*)$_2$(*dmb*)]$^+$ complex. Their emission at 298 K is mainly ^{3}MLCT$_{Ir(ppy)\rightarrow NN}$ and is energetically tunable by ligand modification. [Ir(*Fppy*)$_2$(*dmb*)]$^+$ showed distinguished emission features due to a contribution of triplet ligand-centered excited state of *dmb* (^{3}LC$_{dmb}$) in the emitting T_1 state. All four complexes exhibit intense emission, yet the more pronounced mixed character of complex **Ir1** at room temperature induces an impressive high $\phi \approx 1$. The results exposed here show the importance to anticipate the nature of the ground and excited states and their interactions to describe the emission phenomena. The great features provided by Franck−Condon analyses showed that it is a powerful, yet under-utilized, tool

dx.doi.org/10.1021/ic500070s | Inorg. Chem. 2014, 53, 4089−4099

that underlies theory to understand and predict a diverse set of phenomena, and provide quantitative basis into rates or relative rates for radiative and nonradiative decays from spectroscopic measurements.

The dramatic changes in emission characteristics with temperature observed for these complexes may allow them to be employed in temperature sensors similar to an earlier observation by Fischer et al.[6] Their intense emissions and color variations also make them potential candidates for light-emitting devices that cover a considerable range and are appealing visually as shown in Figure 10.

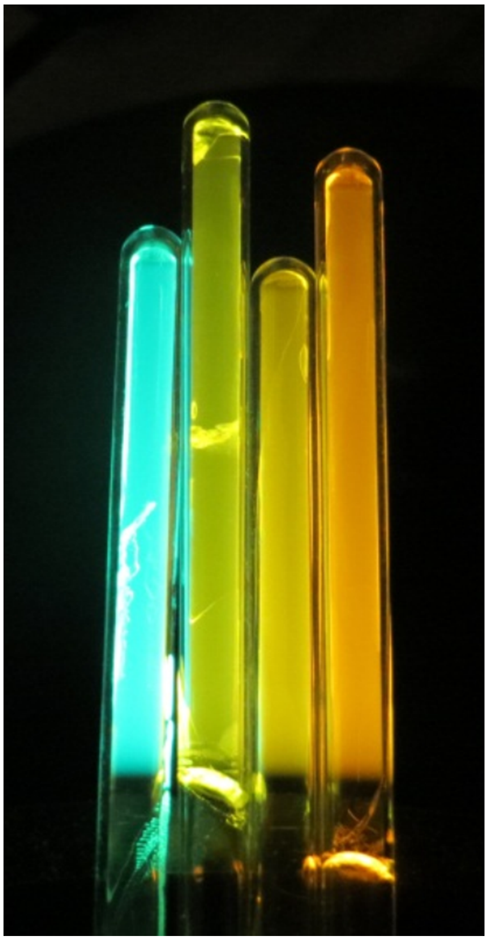

Figure 10. Color array from **Ir1** to **Ir4**.

■ ASSOCIATED CONTENT

Supporting Information

[1]H NMR spectrum of complex **Ir1**, complete TDDFT data and cyclic voltammograms for the four complexes, and Franck–Condon spectral fittings for *dmb* and *Fppy*. This material is available free of charge via the Internet at http://pubs.acs.org.

■ AUTHOR INFORMATION

Corresponding Author

*E-mail: neydeiha@iq.usp.br.

Notes

The authors declare no competing financial interest.

■ ACKNOWLEDGMENTS

This work was supported by Fundação de Amparo à Pesquisa do Estado de São Paulo (FAPESP; 2011/10120-8 and 2012/15478-0), and Conselho Nacional de Desenvolvimento Científico e Tecnológico (CNPq). We thank Dr. Manuel A. Mendez for the electrochemical measurements. A.I. acknowledges support from the U.S. Department of Energy, Office of Science, Office of Basic Energy Sciences, under Award Number DE-FG02-06ER15788. M.K.B. acknowledge support from the UNC Energy Frontier Research Center (EFRC) "Center for Solar Fuels", an EFRC funded by the U.S. Department of Energy, Office of Science, Office of Basic Energy Sciences under Award Number DE-SC0001011.

■ REFERENCES

(1) (a) Itokazu, M. K.; Polo, A. S.; Iha, N. Y. M. *J. Photochem. Photobiol., A* **2003**, *160*, 27–32. (b) Evans, R. C.; Douglas, P.; Winscom, C. J. *Coord. Chem. Rev.* **2006**, *250*, 2093–2126. (c) Lowry, M. S.; Bernhard, S. *Chem.—Eur. J.* **2006**, *12*, 7970–7977. (d) Polo, A. S.; Itokazu, M. K.; Murakami Iha, N. Y. *J. Photochem. Photobiol., A* **2006**, *181*, 73–78. (e) Marin, V.; Holder, E.; Hoogenboom, R.; Schubert, U. S. *Chem. Soc. Rev.* **2007**, *36*, 618–635. (f) Chou, P.-T.; Chi, Y. *Chem.—Eur. J.* **2007**, *13*, 380–395. (g) Santos, G.; Fonseca, F.; Andrade, A. M.; Patrocínio, A. O. T.; Mizoguchi, S. K.; Murakami Iha, N. Y.; Peres, M.; Monteiro, T.; Pereira, L. *Phys. Status Solidi A* **2008**, *205*, 2057–2060. (h) Santos, G.; Fonseca, F. J.; Andrade, A. M.; Patrocínio, A. O. T.; Mizoguchi, S. K.; Iha, N. Y. M.; Peres, M.; Simões, W.; Monteiro, T.; Pereira, L. *J. Non-Cryst. Solids* **2008**, *354*, 2571–2574. (i) You, Y.; Park, S. Y. *Dalton Trans.* **2009**, 1267–1282. (j) Mizoguchi, S. K.; Patrocínio, A. O. T.; Murakami Iha, N. Y. *Synth. Met.* **2009**, *159*, 2315–2317. (k) Ulbricht, C.; Beyer, B.; Friebe, C.; Winter, A.; Schubert, U. S. *Adv. Mater.* **2009**, *21*, 4418–4441. (l) Mizoguchi, S. K.; Santos, G.; Andrade, A. M.; Fonseca, F. J.; Pereira, L.; Murakami Iha, N. Y. *Synth. Met.* **2011**, *161*, 1972–1975. (m) Hu, T.; He, L.; Duan, L.; Qiu, Y. *J. Mater. Chem.* **2012**, *22*, 4206–4215.

(2) (a) Demas, J. N.; Harris, E. W.; Flynn, C. M.; Diemente, D. *J. Am. Chem. Soc.* **1975**, *97*, 3838–3839. (b) Demas, J. N.; Harris, E. W.; McBride, R. P. *J. Am. Chem. Soc.* **1977**, *99*, 3547–3551. (c) Gao, R.; Ho, D. G.; Hernandez, B.; Selke, M.; Murphy, D.; Djurovich, P. I.; Thompson, M. E. *J. Am. Chem. Soc.* **2002**, *124*, 14828–14829.

(3) (a) Shao, F.; Barton, J. K. *J. Am. Chem. Soc.* **2007**, *129*, 14733–14738. (b) Elias, B.; Shao, F.; Barton, J. K. *J. Am. Chem. Soc.* **2008**, *130*, 1152–1153.

(4) (a) Lo, K. K.-W.; Chung, C.-K.; Zhu, N. *Chem.—Eur. J.* **2003**, *9*, 475–483. (b) Hsieh, J.-M.; Ho, M.-L.; Wu, P.-W.; Chou, P.-T.; Tsai, T.-T.; Chi, Y. *Chem. Commun.* **2006**, 615–617.

(5) (a) Kano, K.; Matsumoto, H.; Yoshimura, Y.; Hashimoto, S. *J. Am. Chem. Soc.* **1988**, *110*, 204–209. (b) Green, J. H.; Kumar, R.; Seudeal, N.; Tuck, D. G. *Inorg. Chem.* **1989**, *28*, 123–127. (c) Lowry, M. S.; Goldsmith, J. I.; Slinker, J. D.; Rohl, R.; Pascal, R. A.; Malliaras, G. G.; Bernhard, S. *Chem. Mater.* **2005**, *17*, 5712–5719. (d) Sato, S.; Morikawa, T.; Kajino, T.; Ishitani, O. *Angew. Chem., Int. Ed.* **2013**, *52*, 988–992.

(6) (a) Fischer, L. H.; Stich, M. I. J.; Wolfbeis, O. S.; Tian, N.; Holder, E.; Schäferling, M. *Chem.—Eur. J.* **2009**, *15*, 10857–10863. (b) Fischer, L. H.; Borisov, S. M.; Schaeferling, M.; Klimant, I.; Wolfbeis, O. S. *Analyst* **2010**, *135*, 1224–1229.

(7) (a) Baldo, M. A.; O'Brien, D. F.; You, Y.; Shoustikov, A.; Sibley, S.; Thompson, M. E.; Forrest, S. R. *Nature* **1998**, *395*, 151–154. (b) Adachi, C.; Baldo, M. A.; Thompson, M. E.; Forrest, S. R. *J. Appl. Phys.* **2001**, *90*, 5048–5051. (c) Kwon, S.; Wee, K.-R.; Kim, J. W.; Kang, S. O. *Appl. Phys. Lett.* **2010**, *97*, 023309–3.

(8) (a) Parker, S. T.; Slinker, J. D.; Lowry, M. S.; Cox, M. P.; Bernhard, S.; Malliaras, G. G. *Chem. Mater.* **2005**, *17*, 3187–3190. (b) Bolink, H. J.; Cappelli, L.; Coronado, E.; Parham, A.; Stössel, P. *Chem. Mater.* **2006**, *18*, 2778–2780. (c) Nazeeruddin, M. K.; Wegh, R.

T.; Zhou, Z.; Klein, C.; Wang, Q.; De Angelis, F.; Fantacci, S.; Grätzel, M. *Inorg. Chem.* **2006**, *45*, 9245−9250. (d) Bolink, H. J.; Cappelli, L.; Coronado, E.; Grätzel, M.; Ortí, E.; Costa, R. D.; Viruela, P. M.; Nazeeruddin, M. K. *J. Am. Chem. Soc.* **2006**, *128*, 14786−14787. (e) Su, H. C.; Fang, F. C.; Hwu, T. Y.; Hsieh, H. H.; Chen, H. F.; Lee, G. H.; Peng, S. M.; Wong, K. T.; Wu, C. C. *Adv. Funct. Mater.* **2007**, *17*, 1019−1027. (f) Slinker, J. D.; Rivnay, J.; Moskowitz, J. S.; Parker, J. B.; Bernhard, S.; Abruna, H. D.; Malliaras, G. G. *J. Mater. Chem.* **2007**, *17*, 2976−2988. (g) Su, H.-C.; Chen, H.-F.; Fang, F.-C.; Liu, C.-C.; Wu, C.-C.; Wong, K.-T.; Liu, Y.-H.; Peng, S.-M. *J. Am. Chem. Soc.* **2008**, *130*, 3413−3419. (h) Rothe, C.; Chiang, C.-J.; Jankus, V.; Abdullah, K.; Zeng, X.; Jitchati, R.; Batsanov, A. S.; Bryce, M. R.; Monkman, A. P. *Adv. Funct. Mater.* **2009**, *19*, 2038−2044. (i) Fernández-Hernández, J. M.; Yang, C.-H.; Beltrán, J. I.; Lemaur, V.; Polo, F.; Fröhlich, R.; Cornil, J.; De Cola, L. *J. Am. Chem. Soc.* **2011**, *133*, 10543−10558. (j) Costa, R. D.; Ortí, E.; Bolink, H. J.; Monti, F.; Accorsi, G.; Armaroli, N. *Angew. Chem., Int. Ed.* **2012**, *51*, 8178−8211.

(9) Smith, A. R. G.; Burn, P. L.; Powell, B. J. *ChemPhysChem* **2011**, *12*, 2429−2438.

(10) (a) Nozaki, K. *J. Chin. Chem. Soc.* **2006**, *53*, 101−112. (b) Obara, S.; Itabashi, M.; Okuda, F.; Tamaki, S.; Tanabe, Y.; Ishii, Y.; Nozaki, K.; Haga, M.-a. *Inorg. Chem.* **2006**, *45*, 8907−8921. (c) De Angelis, F.; Fantacci, S.; Evans, N.; Klein, C.; Zakeeruddin, S. M.; Moser, J.-E.; Kalyanasundaram, K.; Bolink, H. J.; Grätzel, M.; Nazeeruddin, M. K. *Inorg. Chem.* **2007**, *46*, 5989−6001. (d) Vlček, A., Jr.; Záliš, S. *Coord. Chem. Rev.* **2007**, *251*, 258−287. (e) Ladouceur, S.; Fortin, D.; Zysman-Colman, E. *Inorg. Chem.* **2010**, *49*, 5625−5641. (f) Valore, A.; Cariati, E.; Dragonetti, C.; Righetto, S.; Roberto, D.; Ugo, R.; De Angelis, F.; Fantacci, S.; Sgamellotti, A.; Macchioni, A.; Zuccaccia, D. *Chem.—Eur. J.* **2010**, *16*, 4814−4825.

(11) (a) Dragonetti, C.; Falciola, L.; Mussini, P.; Righetto, S.; Roberto, D.; Ugo, R.; Valore, A.; De Angelis, F.; Fantacci, S.; Sgamellotti, A.; Ramon, M.; Muccini, M. *Inorg. Chem.* **2007**, *46*, 8533−8547. (b) Hisamatsu, Y.; Aoki, S. *Eur. J. Inorg. Chem.* **2011**, *2011*, 5360−5369. (c) Park, H. J.; Kim, J. N.; Yoo, H.-J.; Wee, K.-R.; Kang, S. O.; Cho, D. W.; Yoon, U. C. *J. Org. Chem.* **2013**, *78*, 8054−8064.

(12) (a) Wilde, A. P.; Watts, R. J. *J. Phys. Chem.* **1991**, *95*, 622−629. (b) Tsuboyama, A.; Iwawaki, H.; Furugori, M.; Mukaide, T.; Kamatani, J.; Igawa, S.; Moriyama, T.; Miura, S.; Takiguchi, T.; Okada, S.; Hoshino, M.; Ueno, K. *J. Am. Chem. Soc.* **2003**, *125*, 12971−12979. (c) Sato, H.; Tamura, K.; Taniguchi, M.; Yamagishi, A. *Chem. Lett.* **2009**, *38*, 14−15. (d) Ito, A.; Meyer, T. J. *Phys. Chem. Chem. Phys.* **2012**, *14*, 13731−13745.

(13) (a) Zanoni, K. P. S.; Sanematsu, M. U.; Murakami Iha, N. Y. *Inorg. Chem. Commun.* **2014**, *43*, 162−164. (b) Zanoni, K. P. S.; Kariyazaki, B. K.; Murakami Iha, N. Y.; Ito, A.; Meyer, T. J. 22nd Winter Inter-American Photochemical Society Meeting, Sarasota, FL, 2013. (c) Zanoni, K. P. S.; Kariyazaki, B. K.; Murakami Iha, N. Y.; Ito, A.; Meyer, T. J. 20th International Symposium on the Photophysics and Photochemistry of Coordination Compounds (20th ISPPCC), Traverse City, MI, 2013.

(14) (a) Allen, G. H.; White, R. P.; Rillema, D. P.; Meyer, T. J. *J. Am. Chem. Soc.* **1984**, *106*, 2613−2620. (b) Ito, A.; Kang, Y.; Saito, S.; Sakuda, E.; Kitamura, N. *Inorg. Chem.* **2012**, *51*, 7722−7732.

(15) Nonoyama, M. *Bull. Chem. Soc. Jpn.* **1974**, *47*, 767−768.

(16) Kariyazaki, B. K.; Zanoni, K. P. S.; Murakami Iha, N. Y. 20° Simpósio Internacional de Iniciação Científica USP (20° SIICUSP), 2012.

(17) Lepeltier, M.; Kwok-Ming Lee, T.; Kam-Wing, Lo. K.; Toupet, L.; Le Bozec, H.; Guerchais, V. *Eur. J. Inorg. Chem.* **2005**, *2005*, 110−117.

(18) (a) Knight, T. E.; Goldstein, A. P.; Brennaman, M. K.; Cardolaccia, T.; Pandya, A.; DeSimone, J. M.; Meyer, T. J. *J. Phys. Chem. B* **2010**, *115*, 64−70. (b) Ito, A.; Stewart, D. J.; Fang, Z.; Brennaman, M. K.; Meyer, T. J. *Proc. Natl. Acad. Sci. U.S.A.* **2012**, *109*, 15132−15135. (c) Ito, A.; Stewart, D. J.; Knight, T. E.; Fang, Z.; Brennaman, M. K.; Meyer, T. J. *J. Phys. Chem. B* **2013**, *117*, 3428−3438.

(19) de Mello, J. C.; Wittmann, H. F.; Friend, R. H. *Adv. Mater.* **1997**, *9*, 230−232.

(20) Suzuki, K.; Kobayashi, A.; Kaneko, S.; Takehira, K.; Yoshihara, T.; Ishida, H.; Shiina, Y.; Oishi, S.; Tobita, S. *Phys. Chem. Chem. Phys.* **2009**, *11*, 9850−9860.

(21) Frisch, M. J.; Trucks, G. W.; Schlegel, H. B.; Scuseria, G. E.; Robb, M. A.; Cheeseman, J. R.; Scalmani, G.; Barone, V.; Mennucci, B.; Petersson, G. A.; Nakatsuji, H.; Caricato, M.; Li, X.; Hratchian, H. P.; Izmaylov, A. F.; Bloino, J.; Zheng, G.; Sonnenberg, J. L.; Hada, M.; Ehara, M.; Toyota, K.; Fukuda, R.; Hasegawa, J.; Ishida, M.; Nakajima, T.; Honda, Y.; Kitao, O.; Nakai, H.; Vreven, T.; Montgomery, J. A., Jr.; Peralta, J. E.; Ogliaro, F.; Bearpark, M.; Heyd, J. J.; Brothers, E.; Kudin, K. N.; Staroverov, V. N.; Kobayashi, R.; Normand, J.; Raghavachari, K.; Rendell, A.; Burant, J. C.; Iyengar, S. S.; Tomasi, J.; Cossi, M.; Rega, N.; Millam, N. J.; Klene, M.; Knox, J. E.; Cross, J. B.; Bakken, V.; Adamo, C.; Jaramillo, J.; Gomperts, R.; Stratmann, R. E.; Yazyev, O.; Austin, A. J.; Cammi, R.; Pomelli, C.; Ochterski, J. W.; Martin, R. L.; Morokuma, K.; Zakrzewski, V. G.; Voth, G. A.; Salvador, P.; Dannenberg, J. J.; Dapprich, S.; Daniels, A. D.; Farkas, Ö.; Foresman, J. B.; Ortiz, J. V.; Cioslowski, J.; Fox, D. J. *Gaussian 09*, revision A.1; Gaussian, Inc.: Wallingford, CT, 2009.

(22) (a) Hay, P. J.; Wadt, R. W. *J. Chem. Phys.* **1985**, *82*, 270−283. (b) Wadt, R. W.; Hay, P. J. *J. Chem. Phys.* **1985**, *82*, 284−298. (c) Hay, P. J.; Wadt, R. W. *J. Chem. Phys.* **1985**, *82*, 299−310. (d) Becke, A. D. *J. Chem. Phys.* **1993**, *98*, 5648−5652. (e) Lee, C.; Yang, W.; Parr, R. G. *Phys. Rev. B: Condens. Matter* **1998**, *37*, 785−789.

(23) Dennington, R.; Keith, T.; Millam, J. *GaussView, Version 5*; Semichem Inc.: Shawnee Mission, KS, 2009.

(24) (a) Caspar, J. V.; Westmoreland, T. D.; Allen, G. H.; Bradley, P. G.; Meyer, T. J.; Woodruff, W. H. *J. Am. Chem. Soc.* **1984**, *106*, 3492−3500. (b) Kim, H. B.; Kitamura, N.; Tazuke, S. *J. Phys. Chem.* **1990**, *94*, 7401−7405. (c) Nozaki, K.; Takamori, K.; Nakatsugawa, Y.; Ohno, T. *Inorg. Chem.* **2006**, *45*, 6161−6178.

(25) Parker, C. A.; Rees, W. T. *Analyst* **1960**, *85*, 587−600.

(26) Huang, K.; Rhys, A. *Proc. R. Soc. A* **1950**, *204*, 406−423.

(27) (a) Marcus, R. A. *J. Phys. Chem.* **1989**, *93*, 3078−3086. (b) Hupp, J. T.; Neyhart, G. A.; Meyer, T. J.; Kober, E. M. *J. Phys. Chem.* **1992**, *96*, 10820−10830.

(28) Fylstra, D.; Ladson, L.; Watson, J.; Waren, A. *Interfaces* **1998**, *28*, 29−55.

(29) Baranoff, E.; Curchod, B. F. E.; Monti, F.; Steimer, F.; Accorsi, G.; Tavernelli, I.; Rothlisberger, U.; Scopelliti, R.; Grätzel, M.; Nazeeruddin, M. K. *Inorg. Chem.* **2011**, *51*, 799−811.

(30) Moore, S. A.; Davies, D. L.; Karim, M. M.; Nagle, J. K.; Wolf, M. O.; Patrick, B. O. *Dalton Trans.* **2013**, *42*, 12354−12363.

(31) Lamansky, S.; Djurovich, P.; Murphy, D.; Abdel-Razzaq, F.; Lee, H.-E.; Adachi, C.; Burrows, P. E.; Forrest, S. R.; Thompson, M. E. *J. Am. Chem. Soc.* **2001**, *123*, 4304−4312.

(32) (a) Lever, A. B. P. *Inorg. Chem.* **1990**, *29*, 1271−1285. (b) Fielder, S. S.; Osborne, M. C.; Lever, A. B. P.; Pietro, W. J. *J. Am. Chem. Soc.* **1995**, *117*, 6990−6993. (c) Worl, L. A.; Duesing, R.; Chen, P.; Ciana, L. D.; Meyer, T. J. *J. Chem. Soc., Dalton Trans.* **1991**, 849−858. (d) Juris, A.; Balzani, V.; Barigelletti, F.; Campagna, S.; Belser, P.; von Zelewsky, A. *Coord. Chem. Rev.* **1988**, *84*, 85−277. (e) Caspar, J. V.; Sullivan, B. P.; Meyer, T. J. *Inorg. Chem.* **1984**, *23*, 2104−2109. (f) Kober, E. M.; Marshall, J. L.; Dressick, W. J.; Sullivan, B. P.; Caspar, J. V.; Meyer, T. J. *Inorg. Chem.* **1985**, *24*, 2755−2763.

(33) Strekas, T. C.; Diamandopoulos, P. S. *J. Phys. Chem.* **1990**, *94*, 1986−1991.

(34) Kober, E. M.; Caspar, J. V.; Lumpkin, R. S.; Meyer, T. J. *J. Phys. Chem.* **1986**, *90*, 3722−3734.

(35) (a) Chen, P.; Meyer, T. J. *Inorg. Chem.* **1996**, *35*, 5520−5524. (b) Chen, P.; Meyer, T. J. *Chem. Rev.* **1998**, *98*, 1439−1478. (c) Mochizuki, D.; Sugiyama, M.; Maitani, M. M.; Wada, Y. *Eur. J. Inorg. Chem.* **2013**, *2013*, 2324−2329.

(36) Polo, A. S.; Itokazu, M. K.; Frin, K. M.; de Toledo Patrocínio, A. O.; Murakami Iha, N. Y. *Coord. Chem. Rev.* **2006**, *250*, 1669−1680.

(37) Patrocinio, A. O. T.; Brennaman, M. K.; Meyer, T. J.; Murakami Iha, N. Y. *J. Phys. Chem. A* **2010**, *114*, 12129−12137.